



Interfacial ion transfer and current limiting in neutral-carrier ion-selective membranes: A detailed numerical model



Matthew T. Flavin^{a,b}, Daniel K. Freeman^a, Jongyoon Han^{b,*}

^a Electronics Division, Draper Laboratory, 555 Technology Square, Cambridge, MA 02139, USA

^b Department of Electrical Engineering & Computer Science, Massachusetts Institute of Technology, Cambridge, MA 02139, USA

ARTICLE INFO

Keywords:

Concentration polarization
Dynamic characteristics
Interfacial ion transfer
Electrochemical impedance spectroscopy
Charge-transfer resistance
Butler–Volmer equation

ABSTRACT

Ion selective membrane (ISM) electrodes are widely used for selective ion sensing applications. Recently, new modalities have emerged whose operation involves active electrical polarization of the media, and current theoretical models are unsuitable to predict their behavior beyond near-equilibrium conditions. Here, we apply numerical modeling of physicochemical transport in such systems to study mechanisms of interfacial ion transfer and their role in limiting processes. Importantly, our analysis suggest that membrane-phase complexation (MC) has strong merits as a replacement for interfacial complexation (IC) in theoretical treatments. For our purpose, we have developed a highly detailed model based on Nernst–Planck–Poisson (NPP) with kinetic reactions of first-order. The solutions were derived in terms of logarithmically transformed concentration variables, allowing us to input experimentally determined stability coefficients. A unique process, referred to here as the reaction boundary layer (RBL), is a characteristic of MC, and we found it could have a significant impact on current–voltage (I–V) characteristics and transfer selectivity. Together with other well-known processes such as electrically driven diffusion, the RBL dictates the limits of ISM electrical polarization. Using our model, we demonstrate that operating outside these limits results in ingress of interfering ion species and concurrent loss of transfer selectivity.

1. Introduction

Driven by a consistent stream of innovation, the ion-selective membrane (ISM) has increasingly become a preferred technology for concentration sensing applications [1,2]. The key component of this system, the ionophore, affords the membrane selectivity towards a targeted primary ion through its ability to form a stable complex with that ion.

Over the last two decades, a new generation of ISM-based sensing techniques has emerged. Distinguished as “dynamic” electrochemical modalities, these characteristically involve active electrical polarization of the media [3]. ISM-based amperometry (for which Scanning Electrochemical Microscopy is a specialized application) [4–10], pulse/flash chronopotentiometry [11–15], and coulometry [16–18] have yielded various improvements over traditional potentiostatic ISM sensing. While most commonly employed to measure changes in concentration, devices based on these principles have also the capacity to produce

changes. Investigators have implemented this reverse mode of operation for applications that include selective chemical extraction/isolation [19–22] and electrochemical neuro-modulation [23]. These dynamic modalities, being relatively nascent, lack a detailed theoretical understanding.

In order to advance these technologies, it is crucial that we develop the ability to model the relevant solute transport phenomena accurately. Some behaviors can be studied using simplified bi-ionic models [24–26]. However, in order to evaluate the preeminent limiting factor of ISM operation—interfering ions—some mechanism of interfacial ion transfer must be invoked [27–32]. In this study, we present a highly detailed Nernst–Planck–Poisson (NPP) model comprised of adjacent membrane and aqueous phases with ion transfer mediated by membrane-phase complexation (MC). The system contains several lipophilic and hydrophilic chemical species whose concentrations we solved as logarithmically transformed variables. This transformation allowed us to input experimentally determined stability coefficients (equilibrium

Abbreviations: BV, Butler–Volmer; CV, cyclic voltammetry; CP, concentration polarization; DBL, diffusion boundary layer; EIS, electrochemical impedance spectroscopy; FEM, finite element method; IC, interfacial complexation; ISC, interfacial space charge; ISM, ion-selective membrane; MC, membrane complexation; NPP, Nernst–Planck–Poisson; RBL, reaction boundary layer

* Corresponding author.

E-mail address: jyhan@mit.edu (J. Han).

<https://doi.org/10.1016/j.memsci.2018.10.065>

Received 10 June 2018; Received in revised form 2 October 2018; Accepted 22 October 2018

Available online 03 November 2018

0376-7388/ © 2018 Elsevier B.V. All rights reserved.

Symbols	
a_i	molar activity of solute i
c_i	molar concentration of solute i
c_i^0	initial and bulk concentrations of each solute i in the aqueous phase
c_L^0	total molar concentration of ionophore added to the membrane
c_R^0	total molar concentration of mobile lipophilic counter-ion added to the membrane
c_i^γ	molar concentration of solute i at the edge of the interfacial transition region with (aq) and (org) designating boundaries adjacent to bulk aqueous and membrane phases respectively
d	thickness of membrane layer
E_x	electric field, x–component
D_i	diffusion coefficient for solute i
F	Faraday constant
f_i	molar activity coefficient of solute i with (aq) and (org) designating its bulk values (constants) in aqueous and membrane phases respectively
J_x	total electric current density, x–component
J_0	effective exchange current density from Butler–Volmer equation
J_x^{app}	applied electric current density
$\vec{k}_i, \overleftarrow{k}_i$	forward and backward first-order reaction rate constants for solute i
K_i^{part}	partition coefficient due to differential solubility of solute i for the interface between membrane and aqueous phases
n	number of ionophore molecules that bind to a single ion in a particular complex
$N_{x,i}$	molar flux density of solute i , x–component
R	universal gas constant
R_i	net volume rate of formation of solute i by chemical reaction
r_{RBL}	effective charge-transfer resistance that arises from the reaction boundary layer (RBL)
t	time
T	absolute temperature
T_i	integral transference of membrane for ion i
V^{app}	electric potential applied at a particular boundary
V^0	equilibrium potential from Butler–Volmer equation
V^ρ	phase-boundary potential at an interface between membrane and aqueous phases
z_i	charge number of ion i
α	effective anodic charge-transfer coefficient from Butler–Volmer equation
β_i^n	stability constant for complex comprised of the neutral lipophilic ionophore bound to the ion i in a $1:n$ stoichiometric ratio ¹
δ_{ISC}	characteristic length of the interfacial space-charge region
δ_{N}	length of the Nernst steady diffusion layer
δ_{RBL}	characteristic length of the reaction boundary layer inside the membrane
δ_γ	length of the phase-field transition region
ϵ_r	relative permittivity
ϵ_0	permittivity of free space
τ_{RBL}	characteristic time-scale of reaction boundary layer (RBL) formation
ψ	electric potential
<i>Superscripts and subscripts</i>	
app	externally applied quantities
(aq)	properties and variables characteristic of the aqueous phase
(org)	properties and variables characteristic of the membrane phase
i	index of any solute present in the system
j	index within a subset of ions designated as interfering
L	ionophore
P	primary ion for a particular ionophore-based system
R	mobile lipophilic counter-ion
γ	phase-field transition region at the interface between aqueous and membrane phases ²
ρ	interfacial space-charge region ²

association constants), untenable in previous efforts due to the limits of machine precision. The development of this model enabled us to address dynamic phenomena arising from active electrical polarization.

On the experimental side, electrochemical impedance spectroscopy (EIS) and cyclic voltammetry (CV) are two of the most powerful tools for evaluating the dynamic properties of electrochemical systems. Applied to the ISM, these tools reveal characteristics that we normally associate with electrodes—charge-transfer impedance [33–35] and apparent redox peaks [4,36,37] (derived from EIS and CV respectively). Appropriately, as demonstrated in Refs. [32] and [38], some of these electrode-like characteristics can be replicated in ISM transport models by directly employing Butler–Volmer (BV) formalism. Our analysis, however, indicates that this approach does not capture several important dynamic phenomena. These phenomena will be one of the focuses of this study.

The ISM interface fundamentally differs from the solid–liquid electrode interface for which BV was originally developed—the ISM interface features a continuous liquid–liquid junction. Despite this, articles such as Ref. [38] argue that BV must reflect a singular electrode-like physical process in the ISM, referred to here as interfacial complexation (IC). However, by definition, BV rate constants depend on an electric potential—in this context, the membrane's phase boundary potential. As such, their theory requires that the interfacial electric field exert direct influence on local rate kinetics. While Onsager et al. demonstrated that this type of influence is possible through the Second Wien

Effect, no such phenomena has been observed in this context [48]. As part of our investigation on dynamic phenomena, we will attempt to elucidate how an electric field can influence ISM interfacial kinetics in the absence of a field effect.

Through numerical and analytical evaluation of our model, we demonstrate that MC gives rise to a process we refer to here as the reaction boundary layer (RBL). We discovered that the RBL produces an effective interfacial impedance (and likewise, demonstrates BV current–voltage characteristics) that is observable from simulated EIS results. Thus, MC provides an explanation for the perceived influence of electric field in ISM interfacial kinetics and, likewise, the ISM's electrode-like characteristics. On this basis, we propose that MC, rather than IC, be considered the exclusive mechanism of interfacial ion transfer.

While MC and IC predict similar behaviors under near-equilibrium conditions, our analysis indicates that the RBL can have a significant effect on the transfer characteristics of the membrane under electrical polarization. Effectively, the RBL gives the membrane an intrinsic current limit. Upon increasing magnitude of polarization, the primary ion concentration at the origin of the RBL will diverge further and further from equilibrium. This transpires concurrently with concentration polarization (CP) from other bulk membrane processes such as electrically driven diffusion (see Section 2.6 for a description of limiting processes, four in total). During excessive enrichment or depletion of solutes as the result of any such process, near-equilibrium models lose

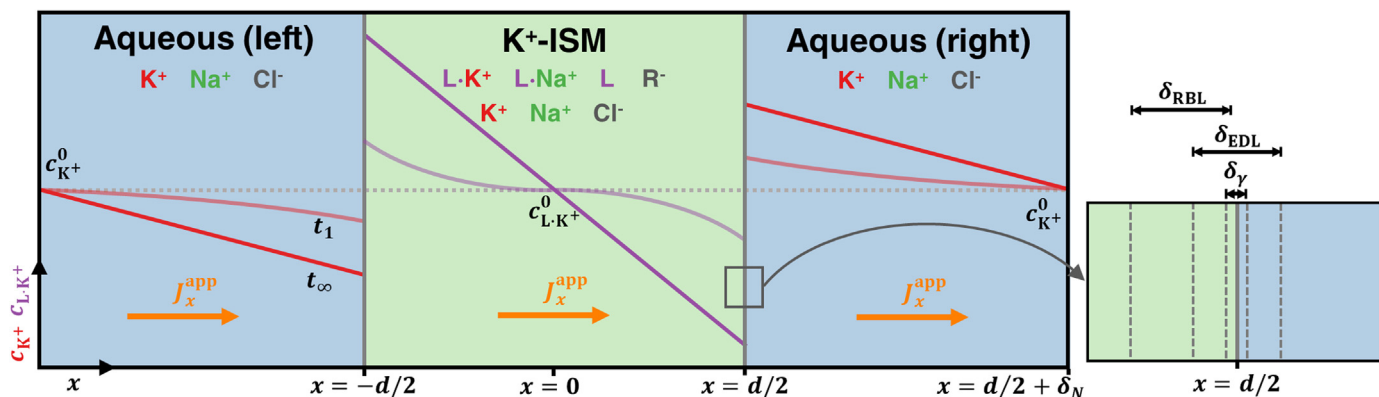


Fig. 1. Schematic of ISM system simulated in this study. Each phase contains hydrophilic solutes— K^+ (primary), Na^+ (interfering), and Cl^- (counter)—as well as lipophilic solutes— L (free ionophore), R^- (mobile lipophilic counter-ion), $L:K^+$, and $L:Na^+$. Due to differential solubility and ionophore reaction, these groups of ions exist in very small concentrations in their respective insoluble phases. Concentration profiles in each phase are depicted here as examples of CP that arise from galvanostatic current, J_x^{app} . The inset zooms in on the phase-boundary region, delineating three boundary layers of interest: the phase transition zone of width δ_γ , the space charge region with characteristic length δ_{ISC} , and the RBL with characteristic length δ_{RBL} .

their fitness. Using solutions to our numerical model, we show here that operation in such regimes causes the membrane to lose transfer selectivity for the primary ion (see Section 2.5 for definition of transfer selectivity).

2. Model description

2.1. Governing equations of solute transport

The time-varying behavior of a physicochemical solute transport system is dictated by continuity, given in this case for 1-D as

$$\frac{\partial c_i}{\partial t} + \frac{\partial N_{x,i}}{\partial x} = R_i, \quad (1)$$

with c_i as the molar concentration, $N_{x,i}$ the x -component of the molar flux density, and R_i the net volume formation rate of chemical reaction of solute i . The energetic preference of a solute for a particular phase, quantifiable from the enthalpy change of solution, relates to the breaking and forming of solvent–solvent and solvent–solute attractions. In our modeling, the activity coefficient was used to define the characteristic solubility of each solute for a particular phase. The molar concentration relates to molar activity, a_i , as

$$a_i = f_i c_i, \quad (2)$$

where f_i is the molar activity coefficient. The gradient of its respective contribution to chemical potential represents a thermodynamic force (of the type described by Onsager [39]) created by differential solubility. In all regions except for the phase transition zones, this force had zero magnitude. For further discussion on differential solubility, see Section 2.2. Chemical flux of each solute from diffusion, migration, and differential solubility is given by the Nernst–Planck equations for dilute solutions:

$$N_{x,i} = -D_i \left(\frac{\partial c_i}{\partial x} + \frac{z_i F}{RT} c_i \frac{\partial \psi}{\partial x} + c_i \frac{\partial \ln f_i}{\partial x} \right), \quad (3)$$

where ψ is the electric potential, D_i is the diffusion coefficient of solute i , and z_i is the charge number of solute i . Meanwhile— F , R , and T hold their usual meanings as Faraday's constant, the universal gas constant, and absolute temperature respectively. The electric potential couples to the space charge density through Poisson's equation:

¹ The superscript is omitted for situations where we assume there is only one characteristic stoichiometric ratio.

² This designates properties intrinsic to the specified region, or variables that are located on the boundaries of it.

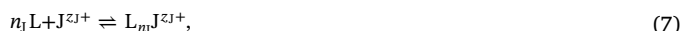
$$\frac{\partial E_x}{\partial x} = -\frac{\partial^2 \psi}{\partial x^2} = \frac{F}{\epsilon_0 \epsilon_r} \sum_{i \in I} z_i c_i, \quad (4)$$

where I is the set of all charged species, E_x is the x -component of the electric field, ϵ_0 is the permittivity of free space, and ϵ_r is the relative permittivity. The electric current density is defined as

$$J_x = F \sum_{i \in I} z_i N_{x,i}, \quad (5)$$

ignoring displacement currents.

In the membrane phase, the following reversible reactions described ionophore binding:



where L is the ionophore, P^{zP+} is the primary ion, J^{zJ+} is an interfering ion, and n_i is number of ionophore molecules that bind to a single ion in a particular complex. Although we could have used any number of interfering ions in our model, this study considered the simple case of one interfering ion. We modeled these reactions according to first-order kinetics:

$$R_{L_n P} = -R_P = \vec{k}_P (c_L)^{n_P} c_P - \bar{k}_P c_{L_n P}, \quad (8)$$

$$R_{L_n J} = -R_J = \vec{k}_J (c_L)^{n_J} c_J - \bar{k}_J c_{L_n J}, \quad (9)$$

$$R_L = n_P R_P + n_J R_J, \quad (10)$$

where \vec{k}_i and \bar{k}_i are the forwards and backwards rate constants respectively. These rate constants relate to the stability coefficient as $\beta_i = \vec{k}_i / \bar{k}_i$.

For a discussion on some of the assumptions taken by our model (related to, for example, ionic size effects, non electrostatic ion–ion interaction, and solvent effects), see Section S-1.

2.2. Continuous 1-D model of transport in aqueous and membrane phases

We applied Eqs. (1–10) to the geometry depicted in Fig. 1. As shown, our system comprised of a membrane of width d placed between two ideal electrodes at distances of δ_N (length of Nernst steady diffusion layer). In each case described in this study, we gave identical conditions to both sides of the membrane. The following describes the Dirichlet boundary conditions applied for each hydrophilic solute in the aqueous phase:

$$c_i\left(x = -\frac{d}{2} - \delta_N\right) = c_i\left(x = \frac{d}{2} + \delta_N\right) = c_i^0. \quad (11)$$

Meanwhile, for lipophilic solutes, we prescribed Dirichlet conditions based on their respective values at equilibrium. The initial conditions for each hydrophilic solute in the aqueous phase were

$$c_i\left(-\frac{d}{2} - \delta_N \leq x \leq -\frac{d}{2}, t = 0\right) = c_i\left(\frac{d}{2} \leq x \leq \frac{d}{2} + \delta_N, t = 0\right) = c_i^0. \quad (12)$$

Finally, we took initial and bulk values for lipophilic solutes in the aqueous phase and all solutes in the membrane phase from solutions to an analytical equilibrium model.

In order to model galvanostatic polarization across the electrodes such that $J_x(x = -d/2 - \delta_N) = J_x^{\text{app}}$, we applied an electric field boundary condition that compensated for diffusion currents. For EIS simulation, we changed the boundary condition to $\psi(x = -d/2 - \delta_N, t) = V^{\text{app}}$, with V^{app} being a time-varying sinusoid. In each case, the electric potential was calculated using the electrode at $x = d/2 + \delta_N$ as its ground reference point. For specific implementation details, see Sections S-2 and S-3.

The differential solubility between the two phases essentially dictates that across their interfacial transition region, the concentrations of solutes must obey $c_i^{\gamma(\text{aq})}/c_i^{\gamma(\text{org})} = K_i^{\text{part}}$. In this report, we use the partition coefficient, K_i^{part} , exclusively in this context. The superscripts (org), (aq), and γ denote properties and variables characteristic of the membrane phase, aqueous phase, and interfacial transition region respectively. Due to numerical issues unique to our logarithmic transformation, we found it necessary to implement solubility as a spatially smooth and continuous property. As per Ref. [40], we used activity coefficients to define characteristic solubilities that varied smoothly between each phase across narrow interfacial transition regions of lengths δ_γ . The distribution of solutes in this implementation was therefore driven by the fourth term in Eq. (3). We chose the values of $f_i^{\text{(org)}}$ and $f_i^{\text{(aq)}}$ such that $f_i^{\text{(org)}}/f_i^{\text{(aq)}} = K_i^{\text{part}}$ (see Section S-4 for relevant derivation).

While not the focus of our study, future investigations might find this implementation valuable for exploring the influence of phase transition regions on interfacial ion transport in ISM systems. As a demonstration of this possible application, we chose our phase distribution function according to the phase-field model employed by Ref. [40] (see Section S-5 for a description). We did not find, however, that the specific choice of distribution function (given a certain δ_γ) had a significant impact on the particular focuses of this study.

2.3. Parameter values

We compiled the parameters used in these simulations, shown in Table 1, from various sources (see Section S-6) for room temperature, $T = 25^\circ\text{C}$. We chose the primary, interfering, and counter ions as $\text{P} = \text{K}^+$, $\text{J} = \text{Na}^+$, and $\text{N} = \text{Cl}^-$. They, along with their respective bulk/initial concentrations, are roughly consistent with a physiological electrolyte.

The diffusion boundary layer (DBL) thickness, δ_N , was estimated to be 300 μm from reported measurements under non-forced hydrodynamic conditions [20]. The membrane had a thickness of $d = 50 \mu\text{m}$, and we based its composition on the one reported in Ref. [41]. We increased the initial concentration of ionophore so that limiting would arise from Type I rather than Type II. This K^+ -selective formulation used Valinomycin as the ionophore and tetrakis(4-chlorophenyl)borate (TpClPB^-) as the mobile lipophilic counter-ion. The binding stability coefficient and complex stoichiometry of the ionophore for the primary ion were taken from Ref. [42] to be $\beta_p = 10^7 \text{ mM}^{-1}$ and $n_p = 1$ respectively. Using the method reported in Ref. [43], we calculated the stability coefficient for the interfering ion in terms of the Nikolsky potentiometric selectivity coefficient. While experimentally determined stability coefficients have been available for the last twenty years, no study has attempted to incorporate them into non-equilibrium transport

models. Stability coefficients of such magnitudes result in very small values, and only by means of logarithmic transformation was our effort possible.

The two types of parameters that could not be determined accurately from the literature were ionophore reaction rates and partition coefficients. The default values used here were chosen based on experimental EIS results, as discussed in the Section 3.1.

2.4. Numerical solution using the finite element method (FEM)

We performed logarithmic transformations on the combined transport and continuity equations of Eqs. (1–3) and (8–10) and re-posed the system as a weak formulation. Ultimately, we solved this using the finite element method (FEM) in COMSOL Multiphysics. For implementation details on the logarithmic transform, weak form, and numerical methods, see Section S-7.

2.5. Integral transference as a quantitative measure of transfer selectivity

Transfer selectivity refers to the ability of the membrane to permit flux of the primary ion while blocking that of all other ions. In this article, we quantify transfer selectivity using the integral transference, T_i , defined according to

$$T_i \equiv \frac{z_i F N_{x,i}}{J_x}, \quad (13)$$

for each ion i [44–47]. Under near equilibrium conditions, integral transference is equivalent to the fraction that a particular ion contributes to the total ionic conductivity (see Section S-8). We can think of integral transference as a dynamic analogue to the Nikolsky selectivity coefficient.

2.6. Membrane limiting processes

We have identified—as stated previously—four critical processes that produce limiting behavior (each depicted schematically in Fig. 2). Types I and II arise from bulk membrane diffusion of the lipophilic counter-ion and free ionophore respectively. Type III arises in the aqueous phase from electrically driven diffusion within a characteristic region referred to as the DBL. Finally, we refer to RBL-based limiting as Type IV. For a background discussion on these processes, see Section S-9.

Generally, the most restrictive solute will determine the characteristic limit of the membrane (i.e. $J_x^{\text{lim}} = \min\{J_x^{\text{lim,R}}, J_x^{\text{lim,L}}, J_x^{\text{lim,aq}}, J_x^{\text{lim,RBL}}\}$). These limits tell us the range of conditions under which the ISM behaves ideally. However, we also want to know the consequences of operating outside of this range. Later, using solutions to our numerical model, we will evaluate the performance of the ISM under non-ideal conditions created by

Table 1
Default model parameters.

i	z_i	$D_i^{\text{(aq)}}$ ($\times 10^{-9}$ m^2/s)	$D_i^{\text{(org)}}$ ($\times 10^{-11}$ m^2/s)	c_i^0 (mM)	$\log \frac{\beta_i^a}{\beta_0}$	$\log \frac{\bar{k}_{i,a}}{k_0}$	$\log K_i^{\text{part}}$
K^+	+1	1.96	1.97	1	7.1	10.3	6
Cl^-	-1	2.01	2.01	101	-	-	8
Na^+	+1	1.35	1.35	100	3.54	10.36	5
TpClPB^-	-1	0.1	0.1	10.3 ^b	-	-	-8
Val	0	0.001	0.1	60 ^b	-	-	-8
Val- K^+	+1	0.001	0.1	-	-	-	-8
Val- Na^+	+1	0.001	0.1	-	-	-	-8

^a Characteristic units, $\beta_0 = 1 \text{ (mM)}^{-n_i}$ and $\bar{k}_0 = 1 \text{ (mM)}^{-n_i \text{ s}^{-1}}$.

^b Total initial concentrations of lipophilic ions added to membrane.

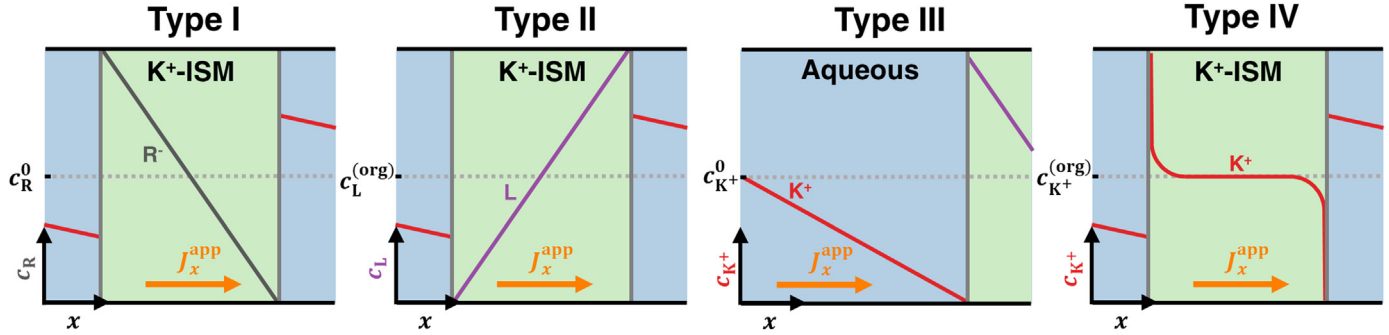


Fig. 2. Depiction of each of the four limiting processes identified in our study.

exceeding those prescribed limits.

3. Results and discussion

3.1. The role of the reaction boundary layer in interfacial ion transfer

As mentioned in the introduction, we implemented interfacial ion transfer in our model as MC. This mechanism partitions ions through the combined effects of differential solubility and volume reaction. For both MC and IC, the following expression holds throughout the bulk of the membrane under equilibrium conditions: $c_{L_n P}^{(org)} = \beta_p (c_L^{(org)})^{np} c_P^{(org)}$. However, MC has an important consequence: a narrow region of CP will develop adjacent to each phase interface when flux is driven across the membrane. This occurs because free ions enter/leave the membrane more quickly than the ionophore can bind/unbind with them. We begin our analysis by examining the structure of the RBL from both analytical and numerical standpoints.

We obtained analytical solutions for two different scenarios: (1) when the size of the RBL is much larger than that of the interfacial space charge region ($\delta_{RBL} \gg \delta_{ISC}$), and (2) when the size of the RBL is much smaller than that of the interfacial space charge region ($\delta_{RBL} \ll \delta_{ISC}$). Starting from Eqs. (1–10) and making use of approximations informed by scale analysis (see Section S-10 for full derivation), we arrive at the following solution for both scenarios:

$$c_P(x = -d/2, t) = c_P^0 + \frac{J_x^{app} \delta_{RBL}}{z_P F} \operatorname{erf}\left(\sqrt{\frac{t}{\tau_{RBL}}}\right), \quad (14)$$

$$\tau_{RBL} \equiv \left[\vec{k}_P (c_L^{(org)})^{np} \right]^{-1}, \quad (15)$$

$$\delta_{RBL} \equiv \sqrt{D_P^{(org)} \tau_{RBL}}, \quad (16)$$

where $c_i^{(org)}$ is the concentration of solute i at a location immediately outside of any interfacial boundary layers. The parameters τ_{RBL} and δ_{RBL} are defined here as the characteristic time and length of the RBL respectively. Intuitively, these become larger and faster, respectively, for a faster reaction rate. If we consider a time-scale that is much less than that of any bulk membrane CP processes (near-equilibrium conditions), note that we can substitute $c_{L_n P}^{(org)} \rightarrow c_R^0/z_P$ and $c_L^{(org)} \rightarrow c_L^0 - \frac{np}{z_P} c_R^0$. As demonstrated in Fig. S-1, solutions to these expressions show excellent agreement with those from the numerical model.

Now, we can determine how the RBL affects the phase-boundary potential. As we know, this potential difference is logarithmically dependent on the free ion concentration inside the membrane. Thus, even an extremely small depletion of that ion adjacent to the interface can have a significant impact. Combining Eq. (14) with the expression for the phase boundary potential, we get the following:

$$J_x^{app} = J_0 \left[\exp\left(\frac{z_P F}{RT} \alpha (V^\rho - V^0)\right) - \exp\left(-\frac{z_P F}{RT} (1 - \alpha)(V^\rho - V^0)\right) \right], \quad (17)$$

$$J_0 \equiv z_P F \sqrt{D_P^{(org)} \vec{k}_P (c_L^{(org)})^{np}} \left(\frac{c_P^{(aq)}}{K_P^{part}} \right)^{1-\alpha} \left(\frac{c_{L_n P}^{(org)}}{\beta_P (c_L^{(org)})^{np}} \right)^\alpha, \quad (18)$$

$$V^0 \equiv \frac{RT}{z_P F} \ln \left(\frac{K_P^{part}}{\beta_P (c_L^{(org)})^{np}} \frac{c_P^{(org)}}{c_P^{(aq)}} \right), \quad (19)$$

where V^ρ is the phase-boundary potential at a single interface (voltage measured across the interfacial space charge region), J_0 is the BV effective exchange current density, and V^0 is the BV equilibrium potential. For each of the two scenarios described above, the effective charge transfer coefficient, α , was determined to be

$$\alpha = \begin{cases} 1, & \delta_{RBL} \gg \delta_{ISC} \\ \frac{\epsilon_r^{(org)} / \delta_{ISC}^{(org)}}{\epsilon_r^{(aq)} / \delta_{ISC}^{(aq)} + \epsilon_r^{(org)} / \delta_{ISC}^{(org)}}, & \delta_{RBL} \ll \delta_{ISC} \end{cases}, \quad (20)$$

where $\delta_{ISC}^{(aq)}$ and $\delta_{ISC}^{(org)}$ are the characteristic lengths of space charge regions in the aqueous and membrane phases respectively. As we can see, Eq. (17) takes on the form of the BV equation. The corresponding small-signal resistance for this process is

$$r_{RBL} = \left. \frac{dV^\rho}{dJ_x^{app}} \right|_{V^\rho = V^0} = \frac{RT}{z_P F} \frac{1}{J_0}. \quad (21)$$

According to the electrode analogy, we can think of this RBL impedance as the membrane's charge-transfer impedance. Note that this r_{RBL} is the resistance of one interface, of which the membrane in our full model has two.

According to the experimental results reported in Ref. [33], this charge-transfer impedance should manifest as a low-frequency arc in an ISM's EIS Nyquist plot. In order to evaluate this behavior, we simulated EIS using the numerical methods described in Section 2.4 (avoiding the approximations that were necessary to derive the closed-form expression in Eq. (21)). As shown in Fig. 3, a low-frequency arc is clearly observable. Appropriate to the relationship described in Eq. (21), this arc diminishes with faster reaction rates.

Interfacial charge relaxation limits how quickly the RBL can influence current–voltage characteristics. In other words, double-layer capacitance effectively short-circuits the RBL resistance stated in Eq. (21). Since charge relaxation is characteristically slower than bulk media polarization (in both aqueous and membrane phases), the RBL and geometric impedances manifest as low and high –frequency arcs respectively in the Nyquist plot.

Finally, we estimated the rate constant, \vec{k}_P , by comparing our simulated charge-transfer impedance to that observed experimentally in Ref. [33]. Our simulation, in accordance with the conditions described in Ref. [33], featured a supporting electrolyte of 50 mM CaCl₂. The purpose of this component was to maintain ionic strength and likewise,

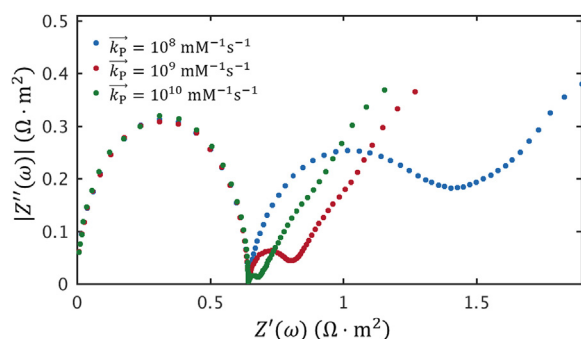


Fig. 3. Nyquist plot for EIS simulated at three different forward reaction rates. A high-frequency arc (associated with bulk media polarization), low-frequency arc (associated with the RBL), and Warburg element can be seen for each.

α , independent of $c_p^{(aq)}$. Ref. [33] chose CaCl_2 specifically because Ca^{2+} has a low affinity for Valinomycin and thus, should not influence the kinetics of K^+ binding. As shown in Fig. 4, both experimental and simulated results agreed that $\alpha = 0.87$. The charge-transfer impedance of membranes, both experimental and simulated, were determined by fitting a Randles equivalent circuit to their respective EIS results. Ultimately, a reaction rate of $\vec{k}_p = 2.3 \cdot 10^{10} \text{mM}^{-1} \text{s}^{-1}$ (given $K_p^{\text{part}} = 10^5$) produced an equivalent resistance.

In Fig. 4, we demonstrate the relationship between aqueous K^+ concentration and charge transfer impedance in a log–log plot for experimental EIS, simulated EIS, and the analytical expression given in Eq. (21) (as the sum of two interfaces). The analytical solution was not independently fitted to the experimental data; rather, we calculated it from the same parameters used in the numerical simulation so that the two solutions could be directly compared. Therefore, we can consider the slight difference between the numerical and analytical plots to be approximation error. Meanwhile, for the given rate constant and partition coefficient, the plots of experimental and simulated are identical.

Altogether, our data suggests that the RBL is the source of the experimental BV impedance previously attributed to IC. In addition, it suggests that non-equilibrium reaction processes can have a significant effect on membrane I–V characteristics. For applications such as dynamic electrochemical sensing, this analysis might allow us to predict an ISM's potentiometric response more accurately.

Furthermore, the RBL has another important effect—a sufficiently large polarization will overcome the selective partitioning of an interface. In Section 3.2, we demonstrate this behavior using solutions to our full numerical model.

As mentioned previously, kinetic rates of ionophore complexation are not currently well understood. However, our results substantiate their potential influence on I–V characteristics and transfer selectivity. Based on our analysis, we propose EIS as a feasible method for the experimental determination of rate constants.

3.2. Loss of transfer selectivity under reaction-limited current regimes

As discussed in Section 2.6, electrically driven flux gives rise to CP in interfacial regions of the membrane. Processes that contribute to this include electrically driven diffusion of charged species, flux driven by interfacial binding and unbinding of the free ionophore, and the RBL. For sufficiently large polarization, we found that each of these processes would ultimately lead to failure of transfer selectivity. We have evaluated this behavior using solutions to our numerical model, focusing specifically on RBL-based limiting in this section and diffusion-based limiting in the following.

While limiting behavior from processes of Types I and II is a product of exhaustive depletion, that from Type IV is a product of excessive enrichment. The enrichment of primary ions (which occurs on the side of the membrane where cations enter) drives the phase-boundary

potential to a higher level (in agreement with Eq. (17)). Our hydrophilic counter-ion (Cl^-), obeying the Nernst equation, consequently rises in concentration throughout the membrane. Thus, for a sufficiently large polarization, the RBL causes the membrane to conduct a higher percentage of nonspecific ions. As we would expect, Fig. 5 demonstrates that slower reaction rates are accompanied by a more restrictive limit on the magnitude of electric current.

As suggested by Eq. (14), the reaction rate required to prevent limiting behavior at a particular current increases for larger stability coefficients. While currents of magnitude $J_x^{\text{app}} \sim 0.1 \text{A/m}^2$ are within the ideally selective regime for this system (where $\beta_p = 10^{7.1} \text{mM}^{-1}$ and $\vec{k}_p = 2.3 \cdot 10^{10} \text{mM}^{-1} \text{s}^{-1}$), such would not be the case for ionophores of higher affinity. ETH 129 (Ca^{2+} -selective), having the largest reported stability coefficient at $\beta_p = 10^{20.2} \text{mM}^{-3}$, would permit significantly little selective flux for the same reaction rate. However, all except for the Ca^{2+} -selective ionophores reported in Ref. [42] had affinities in the range $10^{0.72} \leq \beta_p \leq 10^{8.63}$.

3.3. Loss of transfer selectivity under diffusion-limited current regimes

Limiting behavior, as it arises from electrically driven diffusion in the aqueous phase, has been studied extensively in the field of electro-desalination. Here, we apply similar analysis to that arising from electrically driven diffusion within the membrane. We define a limiting value in this context as the magnitude of electric current required to reduce the concentration of a particular ion to zero on one side of the membrane (as demonstrated in Fig. 6a). We refer to the two regimes characterized by currents of magnitude lesser and greater than this limit as Ohmic and over-limiting respectively. Using an analytical solution, we estimated the limiting value for this system as $J_x^{\text{lim,R}} = 0.0795 \text{A/m}^2$ (see Eqn. S-28). However, as shown in Fig. 6b, some of the over-limiting effects start around 0.06A/m^2 .

Concentration profiles of the mobile lipophilic counter-ion during each of these regimes are displayed in Fig. 6a. While aqueous over-limiting typically occurs through convection-coupled processes, we found selectivity failure to be the prevailing means of over-limiting in the membrane phase. When a sufficiently large electromotive force overcomes the energy barrier created by differential solubility, the membrane permits the ingress of counter and interfering ions. As shown by Fig. 6b, the transition from Ohmic to over-limiting is characterized by a sharp increase in average concentration of Cl^- and, correspondingly, a reduction in selective transference.

According to Eq. (15), the RBL forms very quickly upon initial polarization. In comparison, the time-scales for processes of Types I and II, $\tau_R^{(\text{org})} \sim d^2/\pi^2 D_S^{(\text{org})}$ and $\tau_L^{(\text{org})} \sim d^2/\pi^2 D_L^{(\text{org})}$ respectively, are much slower. Thus, under conditions where Types I or II are the characteristic

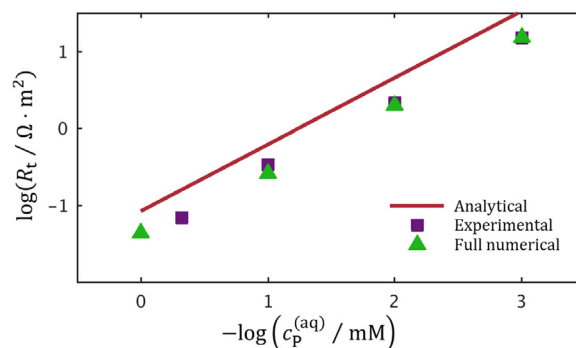


Fig. 4. Logarithmic plot of analytical, experimental (from Ref. [33]), and numerically simulated charge-transfer resistances R_t as a function of K^+ concentration in bathing solution. Both simulated and experimental membranes consisted of $c_R^0 = 6 \text{mM}$, $c_L^0 = 9 \text{mM}$, and an aqueous supporting electrolyte of $50 \text{mM} \text{CaCl}_2$. Both analytical and numerical solutions used the same parameters, with \vec{k}_p determined by fitting numerical to experimental.

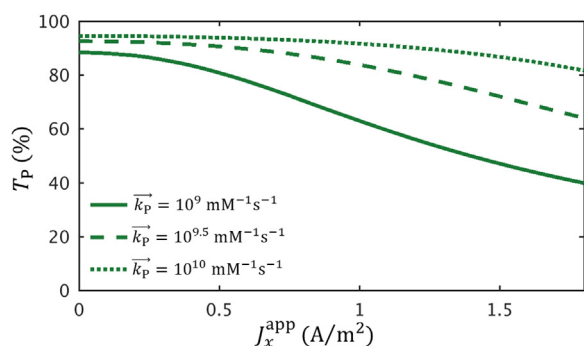


Fig. 5. Impact of concentration enrichment throughout the RBL on transfer selectivity, measured by integral transference for the primary ion, K^+ . Its steady state value is plotted for increasing amplitude of applied current at three different forward reaction rates. We performed these simulations for a membrane of thickness $d = 5\mu\text{m}$ in order to prevent the influence of Types I and II limiting.

limiting process, there will be a window of time where the transfer selectivity of the membrane remains intact. As illustrated in Fig. 7, the numerical solutions to our model demonstrated this behavior.

Therefore, the membrane will operate effectively under two conditions: (1) the applied current is less than the limiting current, or (2) the duration of polarization is less than the time-scale of exhaustive depletion. While analytical expressions (such as Eqs. S-28 and S-29) can sometimes help quantify our operating limits, the numerical simulations described in this section demonstrate what actually happens when those limits are breached.

4. Conclusion

In this study, we presented a highly detailed model of ISM solute transport. Enabled by technical improvements such as the use of logarithmic transformation, we investigated phenomena arising from dynamic ISM operation. Our results shine new light on fundamental mechanisms of interfacial ion transfer. In addition, we demonstrated how these mechanisms could influence selective ion transport.

One of the key phenomena documented in this study was the RBL, which forms when ions are driven through the membrane faster than the ionophore can bind and unbind. Our solutions indicate that MC, of which the RBL is a byproduct, accounts for electrode-like characteristics previously observed in CV and EIS experimental studies. This mechanism is more adherent to first-principles than IC because it does not involve field-dependent reaction rates. For this reason, we propose that MC be considered the exclusive mechanism of interfacial ion transfer.

A key implication of our MC-based model is that the RBL can have a

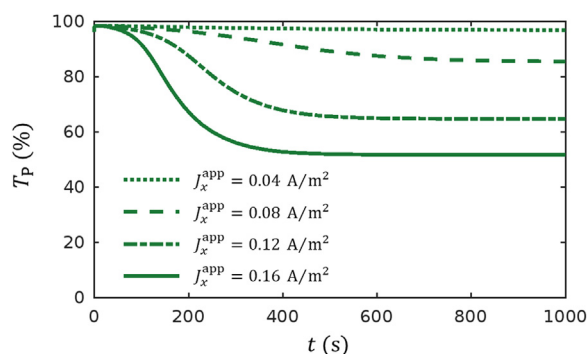


Fig. 7. Temporal evolution of ISM transfer selectivity for the primary ion, K^+ , at several amplitudes of applied current density. This is quantified by the integral transference probed at the location $x = -d/2$.

significant impact on membrane I–V characteristics and transfer selectivity. We predict that this effect would be especially drastic for large stability coefficients, known to be characteristic of some ion–ionophore binding reactions. While the respective rate constants have not yet been reliably measured, our analysis indicates EIS would likely be an effective means of determining such parameters independently.

Along with bulk membrane CP processes such as electrically driven diffusion, the RBL produces a change in the interfacial concentrations of key ions. As a consequence of any such process, sufficiently large (over-limiting) electric currents can drive excessive depletion and enrichment of these ions. Using our numerical model, we found that over-limiting operation results in ingress of interfering ions and loss of transfer selectivity. The onset of this effect can be fast in the case of RBL-based limiting but potentially slow in the case of bulk membrane CP based limiting.

During the investigation of electrically driven ISM transport, our methodology relied heavily on applying concepts from the field of desalination. Although concepts such as transference and limiting conduction have had little exposure in the domain of ISM systems, these are becoming increasingly relevant with the advent of dynamic modalities. Thus, this report has endeavored to bridge some of the gaps between these fields.

The development of these modeling tools facilitates the design and operation of devices used for such applications as dynamic electrochemical sensing and electrochemical modulation. Although this study focuses on ISM electrical polarization (for which our model is particularly advantageous), one could apply our model directly to any mode of operation. Furthermore, the modeling principles described here will be broadly relevant to the treatment of any electrochemical transport system.

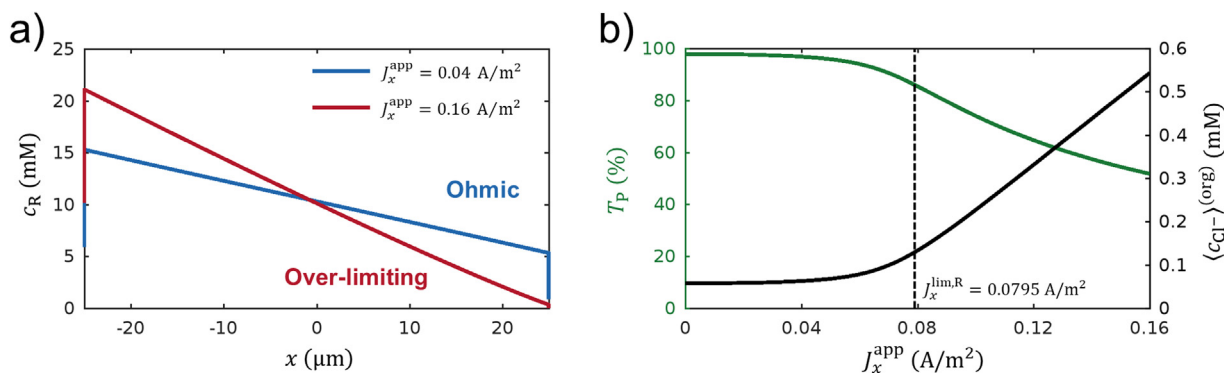


Fig. 6. Limiting behavior arising from electrically driven diffusion within the membrane. (a) Steady-state concentration profiles of lipophilic counter-ion, $TpClPB^-$, during Ohmic and over-limiting regimes. (b) Steady-state transfer characteristics of the membrane for increasing amplitude of current, with the boundary between Ohmic to over-limiting regimes indicated by a dashed line. The integral transference for the primary ion (K^+), and the average membrane concentration of Cl^- are plotted on the left and right axes respectively.

Notes

The authors declare no competing financial interests.

Acknowledgement

The work presented in this article was supported, in part, by the Quick Faculty Innovation Fellowship of MIT, USA. Matthew Flavin was supported by the Draper Laboratory Fellowship, USA.

Appendix A. Supporting information

Supplementary data associated with this article can be found in the online version at doi:10.1016/j.memsci.2018.10.065.

References

- P.C. Gunaratna, W.F. Koch, R.C. Paule, A.D. Cormier, P. Orazio, N. Greenberg, K.M. Connell, A. Malenfant, A.O. Okorodudu, R. Miller, Frozen human serum reference material for standardization of sodium and potassium measurements in serum or plasma by ion-selective electrode analyzers, *Clin. Chem.* 38 (1992) 1459.
- N.F. MacDonald, P.Z. Williams, J.I. Burton, J.G. Batsakis, Sodium and potassium measurements: direct potentiometry and flame photometry, *Am. J. Clin. Pathol.* 76 (1981) 575–577.
- G.A. Crespo, E. Bakker, Dynamic electrochemistry with ionophore based ion-selective membranes, *RSC Adv.* 3 (2013) 25461–25474.
- Y. Kim, S. Amemiya, Stripping analysis of nanomolar perchlorate in drinking water with a voltammetric ion-selective electrode based on thin-layer liquid membrane, *Anal. Chem.* 80 (2008) 6056–6065.
- S. Jadhav, A.J. Meir, E. Bakker, Normal pulse voltammetry as improved quantitative detection mode for amperometric solvent polymeric membrane ion sensors, *Electroanalysis* 12 (2000) 1251–1257.
- M. Senda, H. Katano, M. Yamada, Amperometric ion-selective electrode. Voltammetric theory and analytical applications at high concentration and trace levels, *J. Electroanal. Chem.* 468 (1999) 34–41.
- S. Jadhav, E. Bakker, Voltammetric and amperometric transduction for solvent polymeric membrane ion sensors, *Anal. Chem.* 71 (1999) 3657–3664.
- S. Amemiya, A.J. Bard, Scanning electrochemical microscopy. 40. Voltammetric ion-selective micropipet electrodes for probing ion transfer at bilayer lipid membranes, *Anal. Chem.* 72 (2000) 4940–4948.
- H. Yamada, D. Haraguchi, K. Yasunaga, Fabrication and characterization of a K⁺-selective nanoelectrode and simultaneous imaging of topography and local K⁺ flux Using scanning electrochemical microscopy, *Anal. Chem.* 86 (2014) 8547–8552.
- M. Shen, M.L. Colombo, Electrochemical nanoprobe for the chemical detection of neurotransmitters, *Anal. Methods* 7 (2015) 7095–7105.
- J. Kofler, S. Nau, E.J.W. List-Kratochvil, A paper based, all organic, reference-electrode-free ion sensing platform, *J. Mater. Chem. B* 3 (2015) 5095–5102.
- S. Makarychev-Mikhailov, A. Shvarev, E. Bakker, Pulstrodes: Triple pulse control of potentiometric sensors, *J. Am. Chem. Soc.* 126 (2004) 10548–10549.
- K.L. Gemene, E. Bakker, Direct sensing of total acidity by chronopotentiometric flash titrations at polymer membrane ion-selective electrodes, *Anal. Chem.* 80 (2008) 3743–3750.
- M. Ghahraman Afshar, G.A. Crespo, E. Bakker, Direct ion speciation analysis with ion-selective membranes operated in a sequential potentiometric/time resolved chronopotentiometric sensing mode, *Anal. Chem.* 84 (2012) 8813–8821.
- H. Perera, K. Fordyce, A. Shvarev, Pulsed galvanostatic control of solid-state polymeric ion-selective electrodes, *Anal. Chem.* 79 (2007) 4564–4573.
- E. Grygolowicz-Pawlak, E. Bakker, Thin layer coulometry with ionophore based ion-selective membranes, *Anal. Chem.* 82 (2010) 4537–4542.
- M. Ghahraman Afshar, G.A. Crespo, E. Bakker, Coulometric calcium pump for thin layer sample titrations, *Anal. Chem.* 87 (2015) 10125–10130.
- E. Bakker, Membrane response model for ion-selective electrodes operated by controlled-potential thin-layer coulometry, *Anal. Chem.* 83 (2011) 486–493.
- A. Šlampová, P. Kubáň, P. Boček, Fine-tuning of electromembrane extraction selectivity using 18-crown-6 ethers as supported liquid membrane modifiers, *Electrophoresis* 35 (2014) 3317–3320.
- C. Amatore, S. Szunerits, L. Thouin, J.-S. Warkocz, The real meaning of Nernst's steady diffusion layer concept under non-forced hydrodynamic conditions. A simple model based on Levich's seminal view of convection, *J. Electroanal. Chem.* 500 (2001) 62–70.
- A. Gjelstad, K.E. Rasmussen, S. Pedersen-Bjergaard, Electrokinetic migration across artificial liquid membranes: Tuning the membrane chemistry to different types of drug substances, *J. Chromatogr. A* 1124 (2006) 29–34.
- S. Pedersen-Bjergaard, K.E. Rasmussen, Electrokinetic migration across artificial liquid membranes: New concept for rapid sample preparation of biological fluids, *J. Chromatogr. A* 1109 (2006) 183–190.
- Y.-A. Song, R. Melik, A.N. Rabie, A.M.S. Ibrahim, D. Moses, A. Tan, J. Han, S.J. Lin, Electrochemical activation and inhibition of neuromuscular systems through modulation of ion concentrations with ion-selective membranes, *Nat. Mater.* 10 (2011) 980–986.
- J.M. Zook, J. Langmaier, E. Lindner, Current-polarized ion-selective membranes: The influence of plasticizer and lipophilic background electrolyte on concentration profiles, resistance, and voltage transients, *Sens. Actuators B: Chem.* 136 (2009) 410–418.
- J.M. Zook, R.P. Buck, J. Langmaier, E. Lindner, Mathematical model of current-polarized ionophore-based ion-selective membranes, *J. Phys. Chem. B* 112 (2008) 2008–2015.
- W.E. Morf, E. Pretsch, N.F. De Rooij, Computer simulation of ion-selective membrane electrodes and related systems by finite-difference procedures, *J. Electroanal. Chem.* 602 (2007) 43–54.
- T. Sokalski, W. Kucza, M. Danielewski, A. Lewenstam, Time-dependent phenomena in the potential response of ion-selective electrodes treated by the Nernst–Planck–Poisson model. Part 2: Transmembrane processes and detection limit, *Anal. Chem.* 81 (2009) 5016–5022.
- P. Lingenfelter, I. Bedlechowicz-Sliwakowska, T. Sokalski, M. Maj-Zurawska, A. Lewenstam, Time-dependent phenomena in the potential response of ion-selective electrodes treated by the Nernst–Planck–Poisson model. 1. intramembrane processes and selectivity, *Anal. Chem.* 78 (2006) 6783–6791.
- T. Sokalski, A. Lewenstam, Application of Nernst–Planck and Poisson equations for interpretation of liquid-junction and membrane potentials in real-time and space domains, *Electrochem. Commun.* 3 (2001) 107–112.
- W. Kucza, M. Danielewski, A. Lewenstam, EIS simulations for ion-selective site-based membranes by a numerical solution of the coupled Nernst–Planck–Poisson equations, *Electrochem. Commun.* 8 (2006) 416–420.
- T. Sokalski, P. Lingenfelter, A. Lewenstam, Numerical solution of the coupled Nernst–Planck and Poisson equations for liquid junction and ion selective membrane potentials, *J. Phys. Chem. B* 107 (2003) 2443–2452.
- C. Gabrielli, P. Hemery, P. Letellier, M. Masure, H. Perrot, M.-I. Rahmi, M. Turmine, Investigation of ion-selective electrodes with neutral ionophores and ionic sites by EIS. I. Theory, *J. Electroanal. Chem.* 570 (2004) 275–289.
- S.-L. Xie, K. Cammann, Apparent ion-exchange current densities at valinomycin-based potassium ion-selective PVC membranes obtained with an AC-impedance method, *J. Electroanal. Chem. Interfacial Electrochem.* 229 (1987) 249–263.
- S.-L. Xie, K. Cammann, The determination and characterisation of apparent ion-exchange currents at PVC/water interfaces, *J. Electroanal. Chem. Interfacial Electrochem.* 245 (1988) 117–122.
- E. Lindner, Z. Niegiesz, K. Toth, E. Pungor, T.R. Berube, R.P. Buck, Electrical and dynamic properties of non-plasticized potassium selective membranes, *J. Electroanal. Chem. Interfacial Electrochem.* 259 (1989) 67–80.
- Y. Kim, P.J. Rodgers, R. Ishimatsu, S. Amemiya, Subnanomolar ion detection by stripping voltammetry with solid-supported thin polymeric membrane, *Anal. Chem.* 81 (2009) 7262–7270.
- J. Guo, S. Amemiya, Voltammetric heparin-selective electrode based on thin liquid membrane with conducting polymer-modified solid support, *Anal. Chem.* 78 (2006) 6893–6902.
- R. Ishimatsu, A. Izadyar, B. Kabagambe, Y. Kim, J. Kim, S. Amemiya, Electrochemical mechanism of ion-ionophore recognition at plasticized polymer membrane/water interfaces, *J. Am. Chem. Soc.* 133 (2011) 16300–16308.
- L. Onsager, Reciprocal relations in irreversible processes. I, *Phys. Rev.* 37 (1931) 405–426.
- M.J. Welland, D. Wolf, J.E. Guyer, Multicomponent phase-field model for extremely large partition coefficients, *Phys. Rev. E* 89 (2014) 012409.
- V.V. Cosofret, M. Erdösy, E. Lindner, T.A. Johnson, R.P. Buck, W.J. Kao, M.R. Neuman, J.M. Anderson, Ion-selective microchemical sensors with reduced preconditioning time. Membrane biostability studies and applications in blood analysis, *Anal. Lett.* 27 (1994) 3039–3063.
- Y. Qin, Y. Mi, E. Bakker, Determination of complex formation constants of 18 neutral alkali and alkaline earth metal ionophores in poly(vinyl chloride) sensing membranes plasticized with bis(2-ethylhexyl)sebacate and o-nitrophenyloctylether, *Anal. Chim. Acta* 421 (2000) 207–220.
- E. Bakker, R. Meruva, E. Pretsch, M. Meyerhoff, Selectivity of polymer membrane-based ion-selective electrodes: Self-consistent model describing the potentiometric response in mixed ion solutions of different Charge, *Anal. Chem.* 66 (1994) 3021–3030.
- A.J. Bard, L.R. Faulkner, *Electrochemical Methods: Fundamentals and Applications*, Wiley, 2000.
- S.T. Hwang, K. Kammermeyer, *Membranes in Separations*, Wiley, New York, 1975.
- A.J. Bard, M. Stratmann, E.J. Calvo, *Encyclopedia of Electrochemistry, Interfacial Kinetics and Mass Transport*, Wiley, Weinheim, 2003.
- F.G. Helfferich, *Ion Exchange*, Dover, New York, 1962.
- L. Onsager, Deviations from Ohm's Law in weak electrolytes, *The Journal of Chemical Physics* 2 (1934) 599–615.